Article

Cancer Cell

PF-06463922, an ALK/ROS1 Inhibitor, Overcomes Resistance to First and Second Generation ALK Inhibitors in Preclinical Models

Highlights

- PF-06463922 is a highly potent and selective ALK inhibitor
- PF-06463922 inhibits ALK mutants resistant to current clinical ALK inhibitors
- PF-06463922 is very active against ALK-dependent intracranial tumor models
- PF-06463922 shows a high safety margin in preclinical studies

Authors

Helen Y. Zou, Luc Friboulet, David P. Kodack, ..., Alice T. Shaw, Valeria R. Fantin, Tod Smeal

Correspondence

tod.smeal@pfizer.com

In Brief

Zou et al. show that PF-06463922, an ALK/ROS1 inhibitor, is effective against all known clinical ALK mutants. Moreover, PF-06463922 is effective against brain metastases of EML4-ALK-driven tumors and has high safety margins in preclinical studies.

Zou et al., 2015, Cancer Cell *28*, 70–81
July 13, 2015
http://dx.doi.org/10.1016/j.ccell.2015.05.010

CellPress

CellPress

Cancer Cell
Article

PF-06463922, an ALK/ROS1 Inhibitor, Overcomes Resistance to First and Second Generation ALK Inhibitors in Preclinical Models

Helen Y. Zou,[1,5] Luc Friboulet,[2,5] David P. Kodack,[3,5] Lars D. Engstrom,[1,6] Qiuhua Li,[1] Melissa West,[1] Ruth W. Tang,[1,6] Hui Wang,[1] Konstantinos Tsaparikos,[1] Jinwei Wang,[1] Sergei Timofeevski,[1] Ryohei Katayama,[4] Dac M. Dinh,[1] Hieu Lam,[1] Justine L. Lam,[1] Shinji Yamazaki,[1] Wenyue Hu,[1] Bhushankumar Patel,[3] Divya Bezwada,[3] Rosa L. Frias,[2] Eugene Lifshits,[2] Sidra Mahmood,[2] Justin F. Gainor,[2] Timothy Affolter,[1] Patrick B. Lappin,[1] Hovhannes Gukasyan,[1] Nathan Lee,[1] Shibing Deng,[1] Rakesh K. Jain,[3] Ted W. Johnson,[1] Alice T. Shaw,[2] Valeria R. Fantin,[1] and Tod Smeal[1,*]

[1]Pfizer World Wide Research and Development, 10724 Science Center Drive, San Diego, CA 92121, USA

[2]Department of Medicine, Massachusetts General Hospital Cancer Center, Harvard Medical School, Boston, MA 02114, USA

[3]Department of Radiation Oncology, Edwin L. Steele Laboratory, Massachusetts General Hospital, Harvard Medical School, Boston, MA 02114, USA

[4]Cancer Chemotherapy Center, Japanese Foundation for Cancer Research, Tokyo 135-8550, Japan

[5]Co-first author

[6]Present address: Mirati Therapeutics, 9363 Towne Centre Drive, San Diego, CA 92121, USA

*Correspondence: tod.smeal@pfizer.com

http://dx.doi.org/10.1016/j.ccell.2015.05.010

SUMMARY

We report the preclinical evaluation of PF-06463922, a potent and brain-penetrant ALK/ROS1 inhibitor. Compared with other clinically available ALK inhibitors, PF-06463922 displayed superior potency against all known clinically acquired ALK mutations, including the highly resistant G1202R mutant. Furthermore, PF-06463922 treatment led to regression of EML4-ALK-driven brain metastases, leading to prolonged mouse survival, in a superior manner. Finally, PF-06463922 demonstrated high selectivity and safety margins in a variety of preclinical studies. These results suggest that PF-06463922 will be highly effective for the treatment of patients with ALK-driven lung cancers, including those who relapsed on clinically available ALK inhibitors because of secondary ALK kinase domain mutations and/or brain metastases.

INTRODUCTION

The clinical success of targeting oncogenic tyrosine kinases that are genetically altered through activating mutations, gene translocations, or gene amplification has launched a new era of cancer therapy (Weinstein, 2002). However, acquired resistance is a major limitation to the efficacy of tyrosine kinase inhibitors (TKIs) in the clinic (Bagrodia et al., 2012; Lackner et al., 2012; Rosenzweig, 2012). Crizotinib, a small-molecule inhibitor of the MET, ALK, and ROS1 tyrosine kinases, is highly active in lung cancers harboring chromosomal rearrangements of ALK or ROS1. In ALK-positive non-small-cell lung cancer (NSCLC) patients, crizotinib demonstrated an objective response rate of about 60% and a median progression-free survival of approximately 8 to 11 months (Camidge et al., 2012; Gerber and Minna, 2010; Kwak et al., 2010; Shaw et al., 2013; Solomon et al., 2014c). Similar to the experience with other TKIs, several resistance mechanisms have been observed in patients who relapse on crizotinib. These resistance mechanisms include secondary ALK kinase domain mutations (Choi et al., 2010; Doebele et al., 2012; Katayama et al., 2011, 2012; Sasaki et al., 2011); ALK gene amplification (Doebele et al., 2012; Katayama et al., 2012; Kim et al., 2013); bypass downstream signaling via EGFR (Katayama et al., 2012; Sasaki et al., 2011; Tanizaki et al., 2012), KIT (Katayama et al., 2012), SRC (Crystal et al., 2014), or IGF-1R (Lovly et al., 2014); and pharmacological resistance

Significance

Though the development of ALK inhibitors has changed the course of treatment in NSCLC patients, tumors invariably relapse. Here, we demonstrate the superior properties of the next-generation ALK inhibitor PF-06463922 compared with clinically available ALK inhibitors. PF-06463922 addresses two major mechanisms of clinical relapse, ALK resistance mutations and brain metastasis. Superior potency, selectivity, and physicochemical properties of PF-06462922 are reflected in its ability to achieve potent inhibition of all tested ALK resistance mutations, to penetrate the CNS, and to regress brain metastasis, while having robust safety margins in preclinical studies. PF-06463922 has the potential to treat ALK-driven cancer in both the refractory and the frontline settings.

A

Recombinant ALK kinase domain variant	PF-06463922 Ki GMean (GCI95)	
	nM	n
Wild-type	<0.07	5
L1196M	0.6 (0.5-0.9)	5
G1269A	0.9 (0.3-3.0)	2
1151Tins	0.1	1
G1202R	ND	
L1152R	<0.1	1
S1206Y	0.2	1
C1156Y	<0.1	1
F1174L	<0.1	1

B

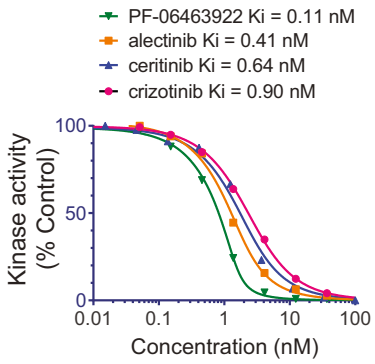

C

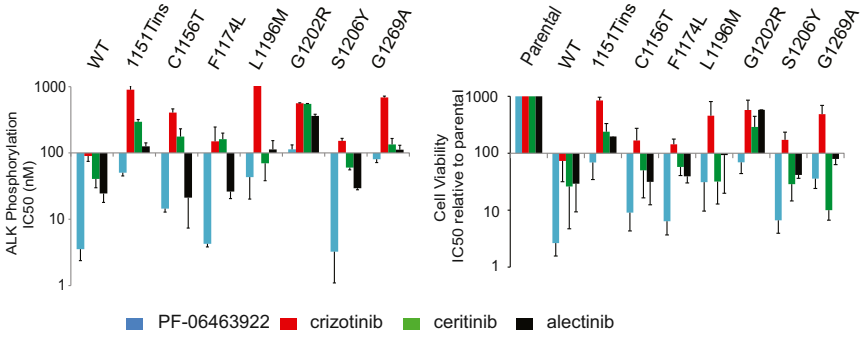

Figure 1. PF-06463922 Is a Potent Inhibitor of Wild-Type ALK and Crizotinib-Resistant ALK Mutants

(A) PF-06463922 in biochemical kinase assays with the indicated recombinant ALK kinase domain constructs. K_i values are geometric means with 95% confidence intervals for n independent measurements.

(B) Biochemical kinase activity of recombinant human wild-type ALK kinase domain treated with the indicated concentrations of PF-06463922, crizotinib, ceritinib, and alectinib. The kinase activity was assayed by a microfluidic mobility shift assay.

(C) IC_{50} values of PF-06463922, crizotinib, ceritinib, and alectinib on ALK phosphorylation (left) and cell viability (right) across different Ba/F3 cell lines expressing wild-type or mutated EML4-ALK relative to parental interleukin-3-dependent Ba/F3 cells.

Values are presented as mean ± SD (n = 3). See also Figure S1 and Table S1.

due to sub-optimal CNS exposure (Costa et al., 2011; Gandhi et al., 2013; Maillet et al., 2013; Weickhardt et al., 2012). Roughly 30% of crizotinib-refractory tumors have been shown to harbor resistance mutations in the ALK kinase domain, including G1269A, L1196M, C1156Y, L1152R, S1206Y, 1151Tins, G1202R, and F1174L (Gainor and Shaw, 2013). Although crizotinib has shown clinical activity against brain metastases (Costa et al., 2013; Kaneda et al., 2013; Kinoshita et al., 2013; Takeda et al., 2013), progression in the brain is particularly common in relapsed patients (Costa et al., 2015; Weickhardt et al., 2012).

Recently, the second-generation ALK inhibitors ceritinib and alectinib have been approved for use in crizotinib-relapsed ALK-fusion-positive NSCLC patients in the United States and for ALK-fusion-positive crizotinib-naive NSCLC patients in Japan, respectively (Chen et al., 2013; Gadgeel et al., 2014; Kinoshita et al., 2012; Shaw et al., 2014a). Although both ALK inhibitors show efficacy in these settings, resistance to both of these inhibitors has emerged. In the case of ceritinib, relapsed tumors often express the ALK mutant G1202R (Friboulet et al., 2014). In the case of alectinib, in addition to G1202R, two ALK resistance mutations (V1180L and I1171T) have been observed (Ignatius Ou et al., 2014; Katayama et al., 2014). Some ALK mutants such as G1202R confer high-level resistance to all clinically available ALK inhibitors (Friboulet et al., 2014; Ignatius Ou et al., 2014; Shaw and Engelman, 2013). Both ceritinib and alectinib have demonstrated activity in brain metastases of crizotinib-relapsed patients. A phase 1 and 2 clinical trial of alectinib showed a CNS response rate of 52% (Gadgeel et al., 2014). Despite the observed CNS activity with these agents, it remains common for patients to relapse with CNS progression. A full understanding of the activity of clinically available ALK inhibitors on brain metastases is still emerging, and we provide a glimpse into mechanisms for their resistance here.

We initiated a drug discovery program with the goal of developing a next-generation ALK inhibitor that is more potent and selective than other known ALK inhibitors (including current second-generation inhibitors), capable of inhibiting all known resistant ALK mutants and able to penetrate the blood-brain barrier (BBB) to achieve therapeutic CNS drug concentrations. PF-06463922, an ATP-competitive small-molecule inhibitor of ALK/ROS1, was successfully discovered by the optimization of physicochemical properties guided by structure-based drug design (Johnson et al., 2014). Here we investigate the preclinical antitumor activity of PF-06463922 in both subcutaneous and intracranial tumor models.

RESULTS

PF-06463922 Has Sub-nanomolar Biochemical and Nanomolar Cellular Potency against Wild-Type and Crizotinib-Resistant ALK Mutants

PF-06463922 is a potent, reversible, ATP-competitive inhibitor of recombinant ALK kinase (Figure S1A). In biochemical assays, PF-06463922 inhibited the catalytic activity of recombinant human wild-type ALK with a mean K_i of <0.07 nM (Figure 1A). In addition, PF-06463922 showed a range of mean K_i values of <0.1 to 0.9 nM against the following crizotinib-resistant ALK mutants: L1196M, G1269A, 1151Tins, F1174L, C1156Y, L1152R, and S1206Y. PF-06463922 was more potent than crizotinib, ceritinib, and alectinib against wild-type ALK in

biochemical studies (Figure 1B). In addition to its high potency against ALK, PF-06463922 has previously demonstrated subnanomolar cell potency against ROS1 (Zou et al., 2015) and demonstrated >100-fold selectivity versus non-target kinases, relative to the ALK^{L1196M} gatekeeper mutant, for >95% of the 206 kinases tested (Johnson et al., 2014).

To directly compare the potencies of PF-06463922, crizotinib, ceritinib, and alectinib in cell assays, NIH 3T3 and Ba/F3 cells were engineered to express either wild-type or the crizotinib-resistant mutants 1151Tins, L1152R, C1156Y, L1196M, G1269A, G1202R, F1174L, or S1206Y (Figures 1C and S1B; Table S1). We observed a strong correlation between drug concentrations required to inhibit ALK phosphorylation and those needed to block ALK-dependent cell proliferation (Figure 1C). PF-06463922 was the most potent inhibitor against all clinically relevant crizotinib-, ceritinib- and/or alectinib-resistant ALK mutants. PF-06463922 showed strong ALK phosphorylation potency against the L1196M (half maximal inhibitory concentration [IC_{50}] = 15–43 nM) and G1269A (IC_{50} = 14–80 nM) ALK mutants, which are two of the most frequently detected crizotinib-resistant mutations observed in the clinic (Doebele et al., 2012; Kim et al., 2013). Furthermore, PF-06463922 demonstrated potent ALK phosphorylation activity against the 1151Tins (IC_{50} = 38–50 nM) and G1202R (IC_{50} = 77–113 nM) ALK mutants that confer a high level of resistance to all second-generation ALK inhibitors (Katayama et al., 2012; Shaw and Engelman, 2013).

PF-06463922 Inhibits ALK-Dependent Cell Growth In Vitro

The activity of PF-06463922 on cell viability and intracellular signaling was examined in H3122 and H2228 ALK-positive lung cancer cell lines. In addition, we examined H3122 cells engineered to overexpress the crizotinib-resistant ALK mutants G1269A and L1196M. Similar to the Ba/F3 cell model, in these cell lines, PF-06463922 was greater than 30-fold more potent than crizotinib with respect to suppressing ALK-dependent signaling and inhibiting cell growth and inducing apoptosis (Figures 2A–2E and S2A–S2D; Table S1). Furthermore, the cell viability of in vitro-derived alectinib-resistant H3122 cells, which contain an endogenous V1180L ALK mutation (Katayama et al., 2014), was sensitive to PF-06463922 via potent inhibition of ALK signaling (Figures 2F and S2E).

The efficacy of PF-06463922 was also examined in cell lines derived from patients with acquired resistance to crizotinib, ceritinib, or alectinib. These cells lines, SNU2535, MGH021-5, and MGH056-1, harbor endogenous EML4-ALK^{G1269A}, SQSTM1-ALK^{G1202R}, and EML4-ALK^{I1171T} mutations, respectively. PF-06463922 exhibited significantly greater cell growth inhibitory potency in these cell lines compared with crizotinib. Cell growth IC_{50} values for PF-06463922 were 47, 63, and 23 nM, respectively, compared with 3,240, 1,046, and 271 nM, respectively, for crizotinib (Figures 2G–2I). These cell growth IC_{50} values correlated closely with the drugs' abilities to inhibit ALK phosphorylation and downstream signaling in these cells (Figures S2F–S2H). Overall, in both the patient-derived and engineered cell lines, PF-06463922 consistently showed greater potency in inhibiting ALK phosphorylation and cell viability compared with clinically available ALK inhibitors.

PF-06463922 Exhibits Potent Antitumor Efficacy In Vivo, and Its Pharmacokinetic-Pharmacodynamic Relationship in These Models

PF-06463922 was evaluated for its efficacy against subcutaneous growth of parental H3122 EML4-ALK^{WT} and engineered H3122 EML4-ALK^{L1196M}, EML4-ALK^{G1269A}, and NIH 3T3 EML4-ALK^{G1202R} tumors (Figures 3A–3D). In these experiments, PF-06463922 was administered by subcutaneous pump infusion, which better mimics the predicted human pharmacokinetic (PK) profile than oral dosing in mice (data not shown). Treatment with PF-06463922 led to a dose-dependent antitumor effect ranging from tumor growth inhibition (TGI) to tumor regression. The effect on tumor growth was consistent with its ability to dose-dependently inhibit ALK phosphorylation. A maximal effect of >95% inhibition of ALK phosphorylation was achieved in each of the models, and this resulted in tumor regression ranging from 35% to 77% (Figure 3; Table S2). Of note, PF-06463922 significantly inhibited tumor growth in crizotinib-resistant models harboring mutant ALK, including the most resistant G1202R mutant.

A simple direct response PK-pharmacodynamic (PD) modeling analysis (Mager et al., 2003) was conducted to elucidate the relationship between PF-06463922 plasma concentration, inhibition of ALK phosphorylation, and suppression of tumor growth. The Hill equation showed reasonable fits for both inhibition of ALK phosphorylation and antitumor efficacy (Figures S3A–S3D). The PK, PD, TGI, and Hill equation parameters of PF-06463922 from these studies are summarized in Tables S2 and S3, and the efficacious concentration (Ceff) values derived from the Hill function analyses are summarized in Table S4. To summarize, the Ceff values for tumor stasis (100% TGI) were determined to be 6.5 nM in the H3122 EML4-ALK^{WT} tumor model, 38 nM in the H3122 EML4-ALK^{G1269A} model, 68 nM in the H3122 EML4-ALK^{L1196M} model, and 165 nM in the 3T3 EML4-ALK^{G1202R} model. The estimated half maximal effective concentrations for inhibiting ALK phosphorylation were comparable to the Ceff values for tumor stasis of each corresponding ALK fusion (Table S4). The Ceff (68 nM free) determined for the H3122 EML4-ALK^{L1196M} model with PF-06463922 administered by infusion is similar to the Ceff (51 nM free) determined using the oral route (Yamazaki et al., 2014). The Ceff values for maximum antitumor response for PF-06463922 correlated closely with the estimated 90% maximal effective concentration values for ALK phosphorylation inhibition in these tumors (Figures S3A–S3D and Table S4).

An oral dosing study in the H3122-EML4-ALK^{L1196M} model demonstrated significant tumor regression (35%) and greater than 95% inhibition of ALK phosphorylation in the 10 mg/kg twice daily (BID) group. The antitumor efficacy of the 10 mg/kg BID oral dosing schedule was similar to that of the 30 mg/kg once daily (QD) group (33% regression), and superior to the 10 mg/kg QD group (3% tumor regression) (Figure S3E). The 10 mg/kg BID group had lower unbound plasma maximal concentration (Cmax) (392 nM) than either the 10 mg/kg QD (1,636 nM) or the 30 mg/kg QD (3,193 nM) group, indicating that the antitumor efficacy of PF-06463922 was not driven by Cmax in this model (Table S2). Collectively, these results indicate that near complete inhibition of ALK phosphorylation (>95%) with prolonged duration during the dosing interval

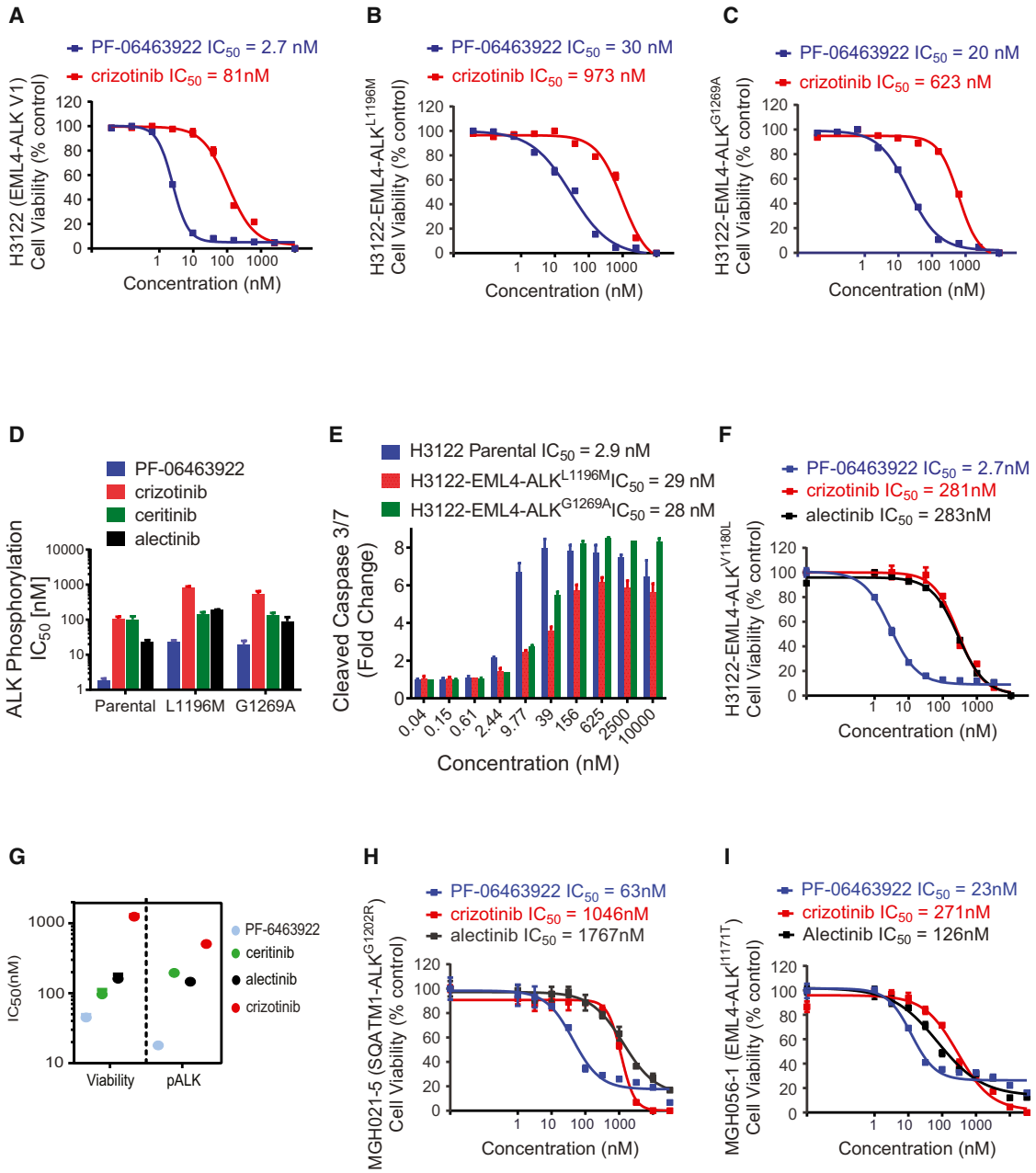

Figure 2. PF-06463922 Potently Inhibits ALK Fusion Wild-Type and Mutant-Mediated Tumor Cell Survival

(A–C) Cell viability assays of H3122 EML4-ALK^{WT} (A), H3122 EML4-ALK^{L1196M} (B), and H3122 EML4-ALK^{G1269A} (C) cells treated with the indicated doses of crizotinib or PF-06463922 for 72 hr. Cell viability was assayed by Cell-Titer-Glo. For (A) to (C), values are presented as mean ± SEM (n = 3).

(D) IC_{50} values of PF-06463922, crizotinib, ceritinib, and alectinib on ALK phosphorylation in H3122 cell lines expressing EML4-ALK^{WT}, EML4-ALK^{L1196M}, and EML4-ALK^{G1269A}. Values are presented as mean ± SEM (n = 3–7).

(E) Cleaved caspase-3/7 induction by PF-06463922 treatment in the three different H3122 cell models. Values are presented as mean ± SD (n = 3).

(F) Cell viability assay of the alectinib-resistant H3122 cell line (EML4-ALK^{V1180L}) treated with the indicated doses of crizotinib, PF-06463922 or alectinib for 72 hr. Values are presented as mean ± SEM (n = 6).

(G) Cell survival and ALK phosphorylation IC_{50} values of PF-06463922, crizotinib, ceritinib, and alectinib on crizotinib-resistant patient-derived cell line SNU2535 (EML4-ALK^{G1269A}). Values are presented as mean ± SEM (n = 3–14).

(H) Cell viability assay of ceritinib-resistant patient-derived cell line MGH021-5 (SQSTM1-ALK^{G1202R}) treated with the indicated doses of crizotinib, PF-06463922, or alectinib for 7 days. Values are presented as mean ± SEM (n = 3).

(I) Cell viability assay of alectinib-resistant patient-derived cell line MGH056-1 (EML4-ALK^{I1171T}) treated with the indicated doses of crizotinib, PF-06463922, or alectinib for 72 hr. Values are presented as mean ± SEM (n = 3).

See also Figure S2.

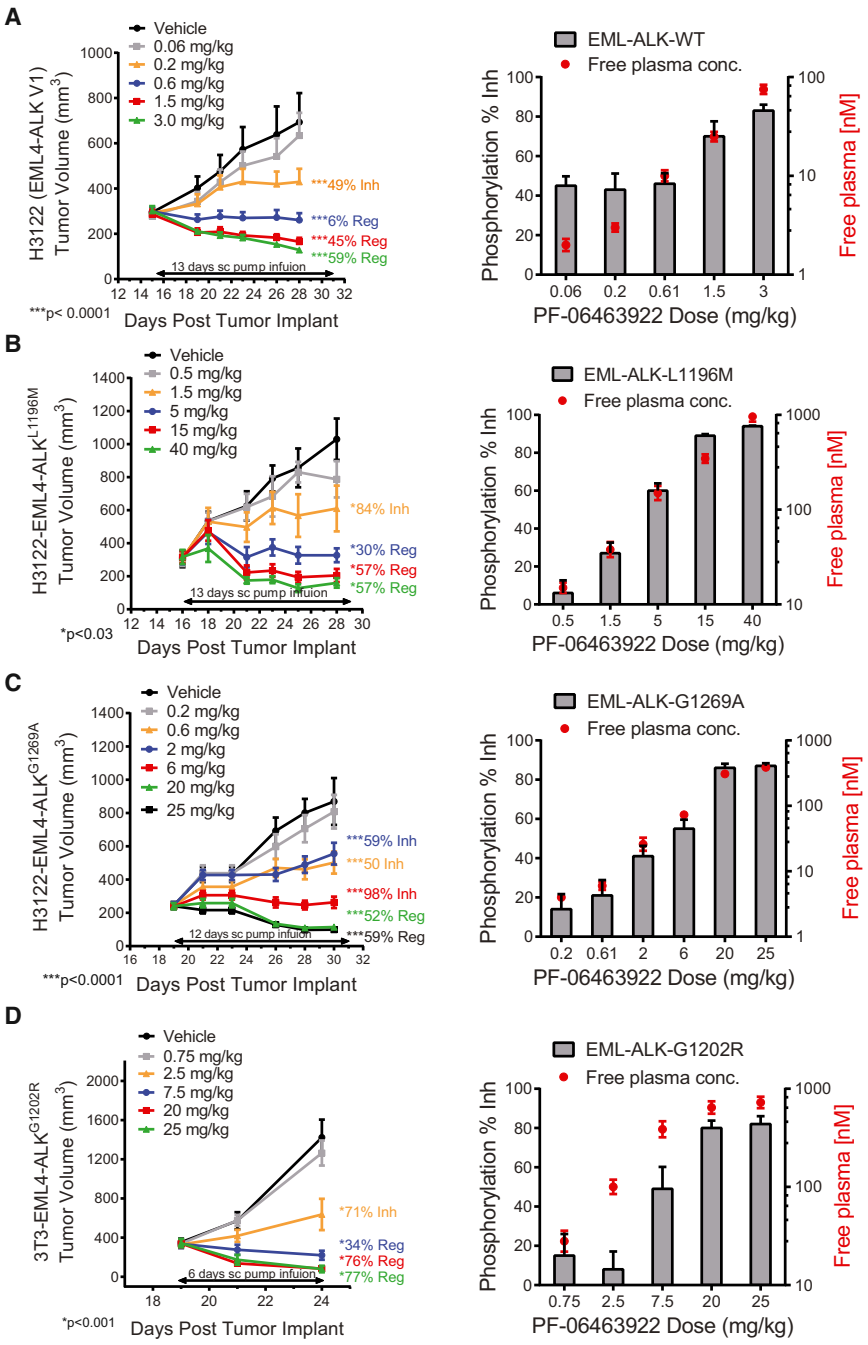

Figure 3. PF-06463922 ALK Target Inhibition PK/PD Relationships in ALK Fusion-Driven Subcutaneous Tumor Xenograft Models in Mice

(A–D) Mini-pump infusion study in H3122 model expressing endogenous EML4-ALK^{WT} (A), H3122 model expressing engineered EML4-ALK^{L1196M} (B), H3122 model expressing engineered human EML4-ALK^{G1269} (C), and 3T3 model expressing engineered human EML4-ALK^{G1202R} (D). Tumor sizes (left) and pALK level and PF-06463922 free plasma concentration (right) of each group are indicated. ALK phosphorylation in tumors was measured at the time of sacrifice following the last tumor volume measurement. The tumors were collected and processed immediately after sacrifice. Tumor volumes, ALK phosphorylation, and plasma concentration values are presented as mean ± SEM (n = 8–12).

See also Figure S3 and Tables S2–S4.

by PF-06463922 is necessary to achieve maximal tumor regression, and PF-06463922 is able to achieve this activity at a relatively low dose.

PF-06463922 Drives Superior TGI In Vivo Compared with Crizotinib

The in vivo efficacy of PF-06463922 was directly compared with that of crizotinib in engineered H3122 models and patient-derived cell lines. Consistent with in vitro data, PF-06463922 showed superior efficacy compared with crizotinib in tumor xenografts derived from H3122 EML4-ALK^{WT} (Figure S4A), H3122 EML4-ALK^{L1196M} (Figure 4A), and H3122 EML4-ALK^{G1269A} cells (Figure S4B). In parallel with tumor growth, PF-06463922 inhibited ALK-mediated signal transduction in tumor tissues collected 3 hr following the final dose of a 4-day treatment regimen to a greater extent than crizotinib. Specifically, ALK, AKT, ERK, STAT3, and S6 phosphorylation was significantly decreased by PF-06463922 in the respective H3122 EML4-ALK models (Figures S4C–S4E). These data corresponded to dose-dependent induction of cleaved caspase-3 levels measured in H3122 EML4-ALK^{L1196M} tumor samples from mice treated with 3 and 10 mg/kg/day of PF-06463922 (Figure 4B). Of note, in H3122 EML4-ALK^{WT} tumor-bearing mice, PF-06463922 showed similar efficacy in inhibiting tumor growth and ALK phosphorylation compared with alectinib (Figures S4A and S4C).

Two ALK-positive patient-derived cell lines were also used to evaluate the in vivo antitumor efficacy of PF-06463922 against wild-type EML4-ALK. MGH051 (EML4-ALK^{WT}) (Figure 4C) was derived from a crizotinib-resistant ALK-positive NSCLC patient (Friboulet et al., 2014). MGH006 (EML4-ALK^{WT}) (Figure S4F) was derived from a crizotinib-naive ALK-positive NSCLC patient (Katayama et al., 2012). Oral administration of PF-06463922 potently suppressed ALK phosphorylation and led to substantial tumor regression of these xenograft models (Figures S4G and S4H).

The antitumor efficacy of PF-06463922 in xenograft models was durable. PF-06463922 suppressed subcutaneous tumor growth longer than 170 days in both MGH051 (EML4-ALK^{WT}) (Figure 4C) and H3122-EML4-ALK^{G1269A} (Figure 4D) and models

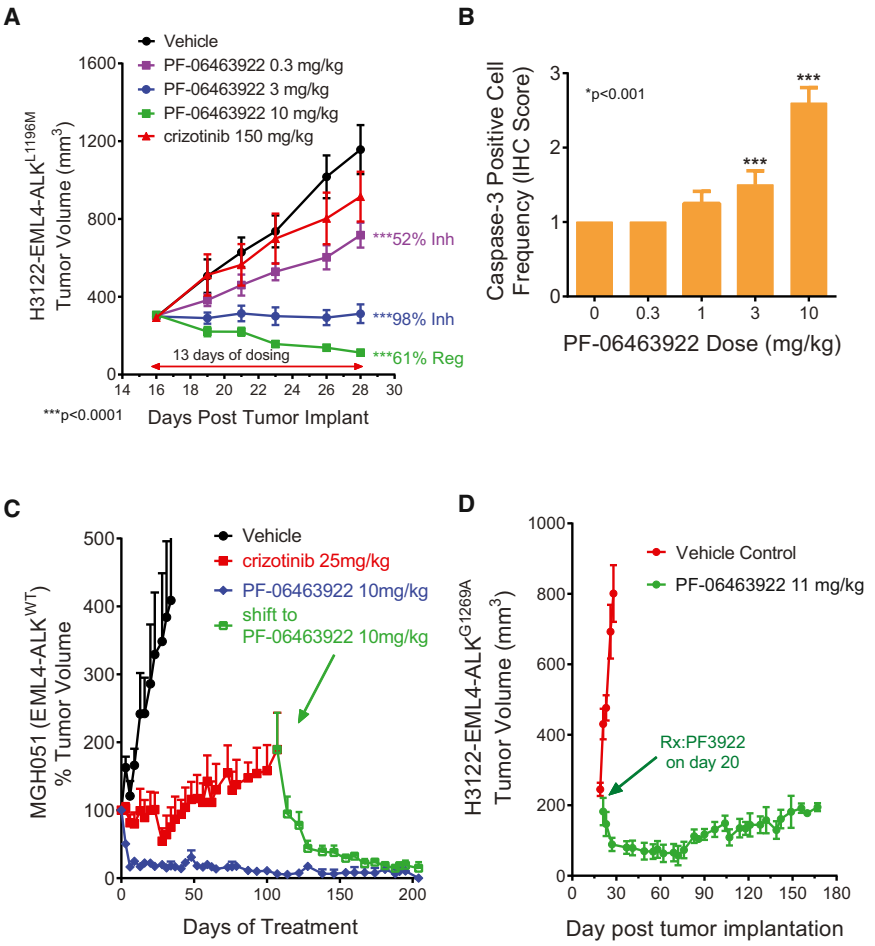

Figure 4. PF-06463922 Antitumor Efficacy in ALK Fusion-Driven Subcutaneous Xenograft Tumor Models in Mice

(A) Subcutaneous tumor growth in the H3122 EML4-ALK^{L1196M} tumor model treated with orally dosed crizotinib 75 mg/kg BID or PF-06463922 0.3 to 10 mg/kg BID for 13 days. Tumor volumes are presented as mean ± SEM (n = 12).

(B) Activated caspase-3-positive cell numbers following 3 days of oral BID administration of PF-06463922 in the H3122-EML4-ALK^{L1196M} model (cf. Figure 4A). Values are expressed as mean ± SEM (n = 7–9).

(C) Long-term subcutaneous tumor growth in the EML4-ALK^{WT} MGH051 crizotinib-resistant patient-derived model treated with crizotinib 25 mg/kg QD or PF-06463922 10 mg/kg BID. The mice treated with crizotinib were shifted to PF-06463922 after 107 days of treatment (arrow). Tumor volumes are presented as mean ± SD (n = 5–12).

(D) Long-term subcutaneous tumor growth of the H3122-EML4-ALKG^{G1269A} tumors treated with PF-06463922 subcutaneous pump infusion at 11 mg/kg/day for 172 days. Tumor volumes are presented as mean ± SEM (n = 5–12).

See also Figure S4.

at drug concentrations predicted to be clinically achievable. Moreover, PF-06463922 induced tumor regression in mice bearing MGH051 tumors that relapsed on crizotinib (Figure 4C).

PF-06463922 Induced Superior Regression of Intracranial EML4-ALK Tumors and Prolonged Mouse Survival Compared with Other Clinically Available ALK Inhibitors

Nearly 50% of ALK-positive NSCLC patients undergoing crizotinib treatment exhibit brain metastasis as the first site of disease progression, and in nearly 80% of these patients, systemic disease is under control (Camidge, 2013; Solomon et al., 2014b). The physicochemical properties of PF-06463922 were specifically optimized to maximize its CNS availability. PF-06463922 demonstrated 21% to 31% free brain drug exposure relative to free plasma concentration in non-tumor-bearing rats and dogs and is predicted to penetrate the intact BBB in humans (Johnson et al., 2014).

To investigate the antitumor efficacy of PF-06463922 in an NSCLC brain metastasis model, we conducted intracranial xenograft studies with EML4-ALK-positive tumor models containing either wild-type EML4-ALK (H3122 or MGH006 cells) or the ALK^{L1196M} gatekeeper mutation (H3122 EML4-ALK^{L1196M} cells). Tumor cells were engineered to express either firefly luciferase or Gaussia luciferase (Gluc) in order to allow noninvasive monitoring of tumor growth in vivo by either whole-body in vivo imaging systems (IVIS) or tail vein blood Gluc activity measurement, respectively.

As shown by MRI (Figures 5A and 5B), IVIS (Figures S5A–S5C) images, and blood Gluc activity measurements over time (Figure 5C), PF-06463922 demonstrated significant antitumor activity against H3122 EML4-ALK^{WT} brain metastases that was superior to either crizotinib or alectinib. In subcutaneous studies, H3122 (EML4-ALK^{WT}) tumors displayed similar sensitivity to PF-06463922 and alectinib (Figure S4A). However, although H3122 brain metastases relapsed between 40 and 120 days after alectinib initiation, PF-06463922 treatment suppressed tumor growth in all mice for the duration of the experiment (160 days). Interestingly, shifting the alectinib-relapsed mice to PF-06463922 induced a second tumor response in those animals, demonstrating that PF-06463922 has superior intracranial efficacy compared with alectinib (Figure 5C). The suppression in brain metastasis growth by PF-06463922 was consistent with better suppression of ALK phosphorylation (Figure 5D). Immunohistochemistry analysis indicated a significant reduction in the Ki67-positive tumor cell number and mitotic index in brain xenografts from mice within the 10 mg/kg BID treatment group (Figures S5C and S5D).

Consistent with the H3122 EML4-ALK^{WT} brain metastasis study, PF-06463922 dose-dependently regressed H3122 EML4-ALK^{L1196M} brain metastases at 5, 10, and 20 mg/kg/day, corresponding to median free brain drug concentrations of 35, 55, and 100 ng/g, respectively (Figures S5E and S5F). In contrast, control-treated mice were euthanized, on average, 11 days after treatment initiation because of declining health attributed to tumor burden.

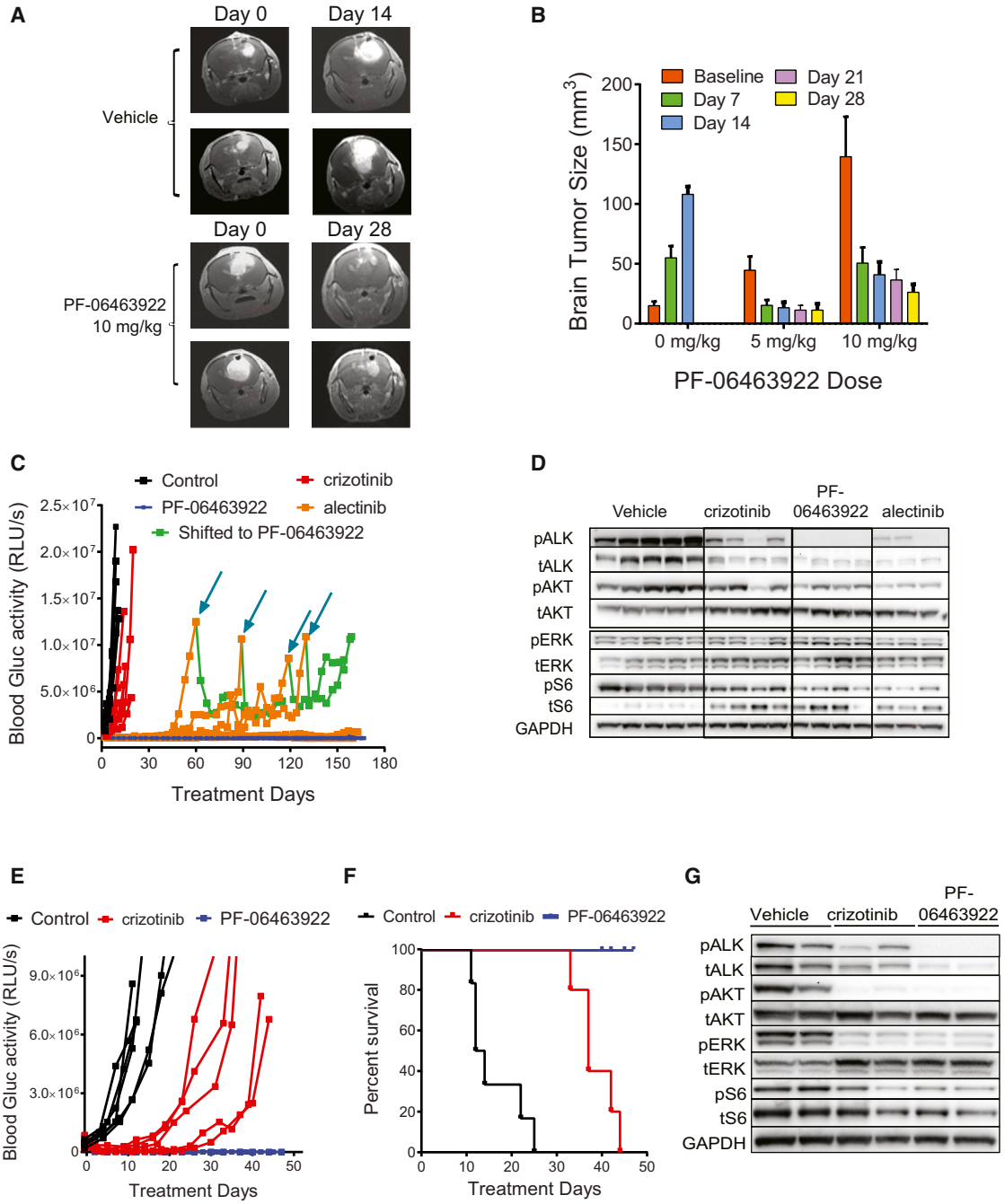

Figure 5. PF-06463922 Antitumor Efficacy in ALK Fusion-Driven Intracranial Tumor Models

(A) Representative magnetic resonance images showing regression of large established H3122 EML4-ALK^{WT} intracranial tumors in mice following PF-06463922 infusion.

(B) Quantitation of brain tumor sizes following PF-06463922 treatment in the H3122 EML4-ALK^{WT} intracranial model shown in (A). Values are presented as mean ± SEM.

(C) Oral dosing of PF-06463922, crizotinib, and alectinib. Long-term brain orthotopic tumor growth of H3122 EML4-ALK^{WT} cells expressing secreted luciferase treated with crizotinib 50 mg/kg QD or alectinib 60 mg/kg QD or PF-06463922 10 mg/kg BID. The mice treated with alectinib were shifted to PF-06463922 at the indicated times (blue arrows).

(D) PD analysis of H3122 EML4-ALK^{WT} brain tumors treated for 3 days and collected 3 hr after last treatment.

(E and F) Brain tumor growth (E) and Kaplan-Meier survival curves ($p < 0.0001$) (F) of MGH006 EML4-ALK^{WT} patient-derived cell line in mice treated orally dosed with crizotinib 100 mg/kg QD or PF-06463922 10 mg/kg/day BID for 42 days.

(G) PD analysis of MGH006 brain tumors treated for 3 days and collected 3 hr after last treatment. Individual blood Gluc activity values are presented for each mouse (n = 5–7 per group).

See also Figure S5.

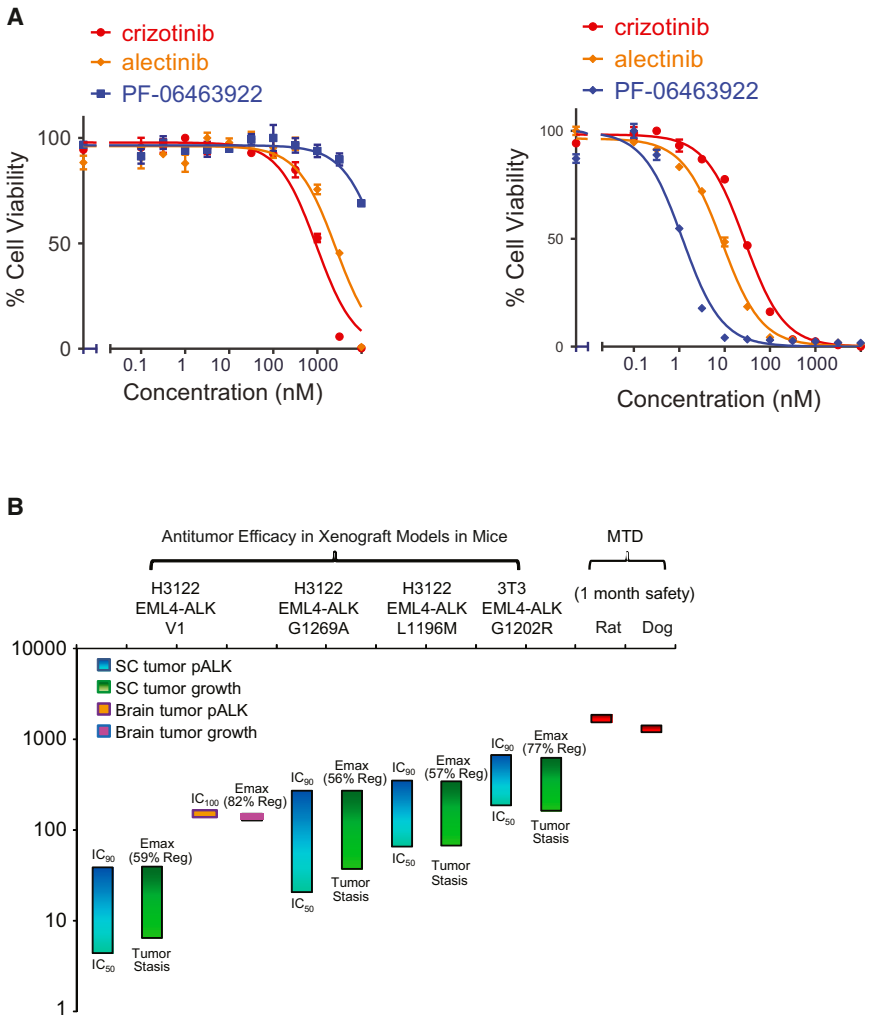

Figure 6. PF-06463922 Preclinical Pharmacology Profile

(A) Cell survival curves of Ba/F3 parental (left) or EML4-ALK^{WT}-expressing cells (right) following treatment for 48 hr with crizotinib, alectinib, or PF-06463922. Cell survival was assayed using Cell-Titer-Glo. Values are presented as mean ± SEM (n = 3).

(B) PF-06463922 preclinical pharmacology profile and safety margin.

See also Figure S6.

We hypothesized that the superior inhibition of brain metastasis growth, attributed to better ALK kinase inhibition, was due to two factors: the enhanced potency of PF-06463922 and/or its increased ability to cross the BBB. To determine which mechanism attributed to its efficacy in our brain metastasis model, we tested an ALK inhibitor, PF-06439015, that possesses 1.5-fold greater potency than PF-06463922 but has poor CNS penetration (Huang et al., 2014; Johnson et al., 2014). Continued subcutaneous infusion of PF-06463922 (6–12 mg/kg/day) suppressed brain tumor growth better than PF-06439015 (36 mg/kg/day) (Figure S5B). PK analysis from these studies indicated that the brain free fraction of PF-06463922 (0.30 ± 0.13) relative to free plasma concentration was >4-fold higher than that of PF-06439015 (0.07 ± 0.02) in mice bearing intracranial tumors. Similarly, better growth delay in the H3122 EML4-ALK^{L1196M} brain metastasis model was attributed to better drug penetration, as PF-06439015 failed to control their growth as brain tumor drug concentrations reached only 9.5 ng/g (Figures S5E and S5F).

Patient-derived MGH006 cells expressing Gluc were equally sensitive to crizotinib and PF-06463922 in subcutaneous studies (Figure S4F). When grown in the brain, however, PF-06463922 suppressed MGH006 tumor growth longer than crizotinib, leading to a significant improvement in survival (Figures 5E and 5F). Crizotinib delayed MGH006 brain metastasis growth roughly 3-fold compared with control-treated mice, but all mice were euthanized within 45 days after treatment initiation because of neurological defects consistent with large CNS tumors. At this time point, brain metastases from PF-06463922-treated mice were barely detectable and much smaller than when treatment was initiated. Consistent with their effects on brain metastasis growth, PF-06463922 achieved better suppression of ALK phosphorylation compared with crizotinib (Figure 5G). Furthermore, we observed reductions in total ALK levels in both treatment groups, but particularly after treatment with PF-06463922. It has been previously reported that HSP90 binding to ALK-fusion proteins in cells is disrupted by crizotinib treatment (Taipale et al., 2013). This disruption may contribute to the reduction in total ALK-fusion protein levels.

PF-06463922 Demonstrated a Broad Therapeutic Window in Preclinical Studies

PF-06463922 demonstrated antitumor efficacy in both subcutaneous and brain orthotopic xenograft models harboring oncogenic ALK fusions containing either wild-type ALK or crizotinib-resistant ALK mutants at pharmacologically relevant doses. PF-06469322 was well tolerated in mice (lack of significant weight loss) at all doses used in our studies (Figure S6). This safety profile is also reflected by in vitro cell assays. For example, compared with other ALK inhibitors, PF-06463922 demonstrated superior activity against ALK-fusion transformed Ba/F3 cells compared with other ALK inhibitors (Table S1), while displaying less toxicity to parental Ba/F3 cells (IC_{50} > 10 μM) (Figure 6A). This finding is likely due to its high level of selectivity (Johnson et al., 2014).

The lack of toxicity of PF-06463922 in Ba/F3 cells, in combination with its superior potency, suggests that this compound could achieve a strong preclinical safety margin. The preclinical safety profile of PF-06463922 was characterized through

single- and repeat-dose studies of up to 1 month in duration in rats and dogs, as well as safety pharmacology and genetic toxicity studies. The nonclinical safety findings related to PF-06463922 were identified at reasonable exposure margins above the Ceff and represent toxicities that can be monitored and are reversible following a 1 month treatment-free period in rat and dog studies. PF-06463922 achieved a greater than 100-fold therapeutic index when comparing its Ceff (tumor stasis) in the EML4-ALK subcutaneous tumor growth model to its maximal tolerated dose (MTD) in both rats and dogs. The Ceff values derived from our in vivo studies are summarized in Table S4. It is worth mentioning that PF-06463922 achieved a maximal effect for either ALK target inhibition or tumor regression in each of the tested efficacy models at exposure levels that are well below the MTD generated from 1 month dog or rat safety studies (Figure 6B). Because PF-06463922 is a brain-penetrable compound, the potential for adverse CNS effects were tested in repeated dose safety studies as well as in the rat contextual renewal model. No CNS-mediated signals were observed in these studies. Furthermore, the functional observation battery (FOB) assessment was included in the 1 month repeated dose study in the rat (data not shown). FOB is a series of noninvasive observational and interactive measures of CNS and automatic system function (e.g., body temperature, pupil response, gait, locomotor activity). No FOB effects were identified, despite achieving plasma exposures 60-fold higher than the predicted minimal efficacious exposure in humans (51 nM free), defined as the free compound concentration needed to achieve tumor stasis in the H3122 EML4-ALK^{L1196M} model.

DISCUSSION

The discovery of oncogenic ALK fusions and the development of ALK targeted therapies, such as crizotinib, have transformed the course of disease for patients with ALK-driven cancers, particularly those with NSCLC. Patients derive significant benefit from either crizotinib or the second-generation inhibitors alectinib and ceritinib. However, the majority of patients invariably relapse, and limited treatment options remain after relapse.

Here we report preclinical data on PF-06463922, a next-generation ALK inhibitor that is currently in a phase 1 and 2 clinical trial (ClinicalTrials.gov identifier NCT01970865) for ALK or ROS1 fusion-positive NSCLC. In a variety of different ALK inhibitor resistant models, PF-06463922 demonstrated broad activity across ALK resistant mutations, including G1202R, which is the most refractory mutation identified to date. G1202R has rarely been reported in the setting of crizotinib resistance but is emerging as a common resistant mutation to the second-generation ALK inhibitors ceritinib (Friboulet et al., 2014) or alectinib (Ignatius Ou et al., 2014). This is consistent with our preclinical studies showing that G1202R confers broad resistance to first-and second-generation ALK inhibitors.

Although crizotinib has shown clinical activity against brain metastases, the CNS is a common site of relapse for patients on crizotinib (Costa et al., 2013, 2015; Solomon et al., 2014a, 2014c). Mechanisms of resistance in the CNS to crizotinib have not been studied in detail, but one plausible mechanism is the inability of crizotinib to achieve therapeutic concentrations in the CNS compartment. Consistent with this notion, a case report showed low levels of crizotinib in the cerebrospinal fluid of a patient who had relapsed with brain metastases (Costa et al., 2011). Poor brain penetration of crizotinib is likely due to its high efflux by P-glycoprotein (PGP) (Johnson et al., 2014). Second-generation ALK inhibitors have shown moderate CNS activity, including patients who have relapsed on crizotinib (Gadgeel et al., 2014). Similar to crizotinib, ceritinib is a PGP substrate and has limited brain penetration (Shaw et al., 2014b) and therefore responses to ceritinib likely reflect its increased potency. Alectinib, on the other hand, is not a PGP substrate and is associated with an intracranial response rate of 52% (Gadgeel et al., 2014). Nevertheless, patients treated with either ceritinib or alectinib still relapse with brain metastases, highlighting the need for a more potent inhibitor with increased CNS availability that, ideally, is not a substrate for PGP. PF-06463922 was specifically designed and optimized to efficiently penetrate the BBB, and as a result it showed ~30% CNS availability in multiple preclinical species. We successfully mimicked the clinical situation in mouse models and showed that ALK fusion tumors, sensitive to crizotinib when growing subcutaneously, were resistant when growing in the brain parenchyma. Furthermore, PF-06463922 demonstrated superior efficacy to after alectinib relapse in our murine models of brain metastasis. PF-06463922 regressed intracranial tumors at doses much lower than the MTD in our preclinical studies. In contrast, a potent ALK inhibitor with low CNS availability (6%) failed to sustain TGI in the same intracranial tumor model, suggesting penetration into the brain metastasis plays a major role in the activity of PF-06463922. Although PF-06463922 provides hope that it will overcome brain metastases that develop in patients who relapse to first- and second-generation ALK inhibitors, data from the ongoing phase 1 study of PF-06463922 will be necessary to evaluate the CNS activity of PF-06463922 in humans, as preclinical studies may not predict brain penetration in humans.

The potency and safety profile, in combination with the penetration into the CNS, of PF-06463922 provides an opportunity to address both acquired and pharmacological mechanisms of drug resistance. Preclinical studies suggest a favorable preclinical safety window for PF-06463922 consistent with the ability to treat patients with drug exposures high enough to inhibit the most recalcitrant G1202R mutant and to reach therapeutic levels in the CNS. Preclinical studies are not always capable of predicting clinical toxicity, so data from the ongoing phase 1 study of PF-06463922 will be critical in understanding the safety margin that PF-06463922 can achieve in humans.

The most immediate impact of PF-06463922 may be on patients in whom previous ALK TKIs have failed, not only in systemic disease but also with brain metastases. Given that PF-06463922 is the most potent and brain-penetrable inhibitor that we tested in our models, whether it should be used as frontline treatment is an intriguing question that awaits clinical investigation. For example, could the frontline use of PF-06463922 lead to more durable responses than sequential therapy in the clinic, as suggested by the sustained responses seen with PF-06463922 in preclinical studies? Finally, if the safety and efficacy of PF-06463922 are confirmed in the clinic, PF-06463922 may serve as an ideal backbone for combination

therapies aimed at overcoming and even preventing the emergence of resistant clones.

EXPERIMENTAL PROCEDURES

Enzyme Assays and Compounds

Recombinant human wild-type and mutant ALK kinase domain proteins (amino acids 1093–1411) were produced in house using baculoviral expression, pre-activated via auto-phosphorylation with MgATP, and assayed for kinase activity using a microfluidic mobility shift assay. The reactions contained 1.3 nM wild-type ALK or 0.2 to 10 nM mutant ALK (appropriate to produce 15%–20% phosphorylation of peptide substrate after 1 hr reaction), 3 μM 5-FAM-KKSRGDYMTMQIG-CONH2, 5 mM $MgCl_2$, and the Km-level of ATP in 25 mM HEPES (pH 7.1). The K_i values were calculated by fitting the percentage conversion to a competitive inhibition equation (GraphPad Prism; GraphPad Software). PF-06463922 and PF-06439015 were synthesized as described in Huang et al. (2014) and Johnson et al. (2014), respectively, and PF-02341066 as described in Cui et al. (2011). The physical properties of PF-06463922 were specifically optimized to maximize CNS availability by controlling molecular weight, lipophilicity, and hydrogen bond donor count.

Cell Culture and Reagents

NCI-H3122 human NSCLC cells were licensed from the National Institutes of Health (NIH). Karpas299 and NIH 3T3 cells were purchased from American Tissue Culture. BaF3 cells were obtained from DSMZ. NCI-H3122 and NCI-H2228 are human lung adenocarcinoma cell lines harboring the EML4-ALK fusion protein variant 1 (V1) and variant 3 (V3a/b), respectively. The SNU2535, MGH056-1, and MGH021-5 NSCLC cell lines were derived from crizotinib-, alectinib-, or ceritinib-relapsed patients and harbor the mutant ALK fusion proteins G1269A, I1171T, and G1202R, respectively. MGH006, MGH051-1, MGH021-5, and MGH056-1 were maintained as previously described (Friboulet et al., 2014; Katayama et al., 2012, 2014; Kim et al., 2013). Cell culture reagents were obtained from Life Technologies. Cells were maintained at 37°C in a humidified atmosphere with 5% to 10% CO_2.

Engineered Cell Line Generation

The target of interest was first cloned into the retroviral vector pMSCV puro or pMSCVhygro. The retroviruses carrying recombinant genes were produced in 293T cells by co-transfection with the pMSCV vectors and the packaging plasmid pCL10A1. The retroviral supernatants were used to transduce NCI-H3122, NIH 3T3, or BaF3 parental cells, and pooled populations were selected with 2 mg/l puromycin or 50 mg/l hygromycin for 5 days.

Cell-Based Kinase Phosphorylation ELISAs

Cells were seeded in 96-well plates in growth media with 0.5% fetal bovine serum and incubated overnight. Compounds were diluted in media without serum, added to the cells, incubated for 1 hr, and then removed by aspirating the media by vacuum suction. Cell lysates were generated and the phospho-ALK (Tyr1604) levels were determined by using the PathScan Phospho-ALK (Tyr1604) Chemiluminescent Sandwich ELISA Kit (Cell Signaling) or PathScan Total ALK Chemiluminescent Sandwich ELISA Kit (Cell Signaling), as described in the manufacturer's protocol. IC_{50} values were calculated by concentration-response curve fitting using a four-parameter analytical method. This phospho-ALK ELISA was also used to determine phosphor-ALK levels in the protein extracts from xenograft tumor samples.

Cell Proliferation Assay

Cells were seeded in 96-well plates in growth media containing 10% fetal bovine serum (FBS) and cultured overnight at 37°C. The following day, serial dilutions of PF-06463922 or appropriate controls were added to the designated wells, and cells were incubated at 37°C for 72 hr. A Cell Titer Glo assay (Promega) was then performed to determine the relative cell numbers. IC_{50} values were calculated by concentration-response curve fitting using a four-parameter analytical method.

Cell Caspase-3/7 Activity Assay

Cells were seeded in 96-well plates at 15,000 cells/well in RPMI media supplemented with 0.5% FBS (Assay Media) and allowed to adhere overnight at 37°C. The following day, 10 mM PF-06463922 was serially diluted in DMSO, and the DMSO dilutions were further diluted in Assay Media and added to the designated wells resulting in a range of serially diluted concentrations of PF-06463922 in the media with 0.5% serum and 0.1% DMSO. The cells were incubated for 24 hr, and the caspase-3/7 activity was measured using the Caspase-Glo 3/7 Assay Kit (Promega), as described in the manufacturer's protocol. IC_{50} values were calculated by concentration-response curve fitting using a four-parameter analytical method.

Animals

Female nu/nu mice aged 5 to 8 weeks were obtained from Charles River. Animals were maintained under clean-room conditions in sterile filter-top cages with Alpha-Dri bedding and housed on HEPA-filtered ventilated racks. Animals received sterile rodent chow and water ad libitum. All animal procedures were performed in compliance with the Institute for Laboratory Animal Research Guide for the Care and Use of Laboratory Animals and the Public Health Service Policy on Human Care of Laboratory Animals. Experiments were approved by the Animal Care and Use Committee at Pfizer La Jolla and by the Institutional Animal Care and Use Committee of Massachusetts General Hospital.

Drug Administration

In all tumor xenograft studies, the compound of interest was administered either orally at 5 to 10 ml/kg using sterile 20-gauge feeding needles (Popper and Sons) or with a subcutaneous Alzet mini-pump (Durect) infusion.

Subcutaneous Tumor Model

The cells were supplemented with 50% Matrigel (BD Biosciences) to facilitate tumor take. Cells (5×10^6 in 100 μl) were implanted subcutaneously into the hind flank region of the mouse and allowed to grow to the designated size prior to the administration of compound for each experiment. Tumor size was determined by measurement with electronic calipers, and tumor volume was calculated as length × width^2 × 0.4.

Intracranial Tumor Model

For injection into the brain, the head of the mouse was fixed with a stereotactic apparatus, and the skull over the left hemisphere of the brain was exposed via skin incision. Using a high-speed air-turbine drill (CH4201S; Champion Dental Products) with a burr tip size of 0.5 mm in diameter, three sides of a square (2.5 mm in length, each side) were drilled through the skull until a bone flap became loose. Using blunt tweezers, the bone flap was pulled back, exposing the brain parenchyma. One hundred thousand cancer cells, diluted in 1 μl PBS, were stereotactically injected into the left frontal lobe of the mice. The bone flap was then placed back into position in the skull and sealed using histocompatible cyanoacrylate glue, and the skin atop the skull was sutured closed. Brain metastatic tumor growth was measured through the use of Gluc, an in vivo secreted reporter expressed by tumor cells and measured in the peripheral blood. In similar models, the blood Gluc activity directly correlated with tumor volume (Kodack et al., 2012).

MRI Study

Magnetic resonance images were acquired with a Bruker 7.0 T scanner with an Avance II console using a 72 mm inside diameter linear birdcage resonator for transmission and a two-element surface coil array for local reception. Pre- and post-contrast T1-weighted fast spin-echo images were acquired. While in the scanner, the temperature and respiratory trace of each mouse were monitored continuously. The isoflurane-oxygen mixture (1.4%–2.0%) was adjusted on the basis of the respiratory rate. The mouse temperature was stabilized by forced-air heating with automatic feedback from a rectal temperature probe. Before post-contrast scans, mice were injected with gadolinium. Injections were timed such that image acquisition coincided with a period of stable tumor contrast, as determined in a pilot study. Tumor volume was calculated by manual segmentation of T1-weighted images using ImageJ software (NIH).

Ex Vivo Target Modulation (PK/PD) Studies

For tissue and plasma processing for PK/PD studies, mice were humanely euthanized, blood and brain tissue samples were collected for PK analysis, and tumors were resected for PD analysis. Plasma and brain samples were analyzed for PF-06463922 concentration using liquid chromatography mass spectrometry analysis. Resected tumors were snap-frozen and pulverized on a liquid nitrogen cooled cryomortar and pestle, and lysed in cold 1X Cell Lysis Buffer (Cell Signaling Technologies). Proteins were extracted from tumor lysate, and protein concentrations were determined using a BSA assay (Pierce). The level of phosphorylated ALK in each tumor sample was determined using the capture ELISA or western blotting method.

Immunoblotting

The immunoblotting method was also used to determine relative kinase phosphorylation status and total protein levels in cells and tumor tissues for the protein of interest. Extracted protein samples from cells or tumor lysates were separated by SDS-PAGE and transferred to nylon membranes, and immunoblotting hybridizations for the proteins of the interest were performed using the corresponding antibodies. Phospho-ERK (T202/Y204), ERK, S6, phospho S6, phospho-AKT (S473 and T308), AKT, phospho-ALK (Y1282/1283), and ALK antibodies were obtained from Cell Signaling Technology. GAPDH was purchased from Millipore.

Statistics

Sample size for in vivo TGI studies was estimated to be about n = 8 to 12 per group to ensure 80% power to capture 70% TGI in a one-sided test on the basis of variability estimate from historical data. Animals were randomized into different treatment groups stratified on their initial tumor size, so the average tumor size for each group was similar at baseline. Standard inclusion and exclusion criteria were used whereby animals were excluded only in rare occasions (such as death) after randomization. Investigators were not blinded to treatment assignment. Because of skewed distribution of the tumor volume data, ANOVA models were fit to the rank-transformed tumor volume. Individual comparisons between treatment groups and vehicle group or among the treatment groups were assessed withone1-sided least significant difference tests and, all under the ANOVA model for ranks.

SUPPLEMENTAL INFORMATION

Supplemental Information includes Supplemental Experimental Procedures, six figures, and four tables and can be found with this article online at http://dx.doi.org/10.1016/j.ccell.2015.05.010.

AUTHOR CONTRIBUTIONS

H.Y.Z., L.F., and D.P.K. contributed to the conception and design of this study, to the acquisition of data, to the analysis and interpretation of data, and to the writing of the manuscript. H.Y.Z. focused primarily on the H3122 and engineered cell lines, on in vitro and in vivo target inhibition and efficacy, and on PKPD relationships in subcutaneous and brain xenograft models. L.F. focused primarily on patient-derived cell line studies, including the biochemical analysis. D.P.K. focused mainly on the brain metastasis studies.

ACKNOWLEDGMENTS

This work was supported by a grant from the NIH (5R01CA164273-02 to A.T.S.). The study was also supported by a grant from the USA Department of Defense Breast Cancer Research Innovator Award W81XWH-10-1-0016 and P01-CA080124 (to R.K.J.). This study was also supported, in part, by Uniting Against Lung Cancer (to L.F.). The authors H.Y.Z., L.D.E., Q.L., M.W., R.W.T., H.W., K.T., J.W., S.T., D.M.D., H.L., J.L.L., S.Y., W.H., T.A., P.B.L., H.G., N.L., S.D., T.W.J., V.R.F., and T.S. are employees and shareholders of Pfizer, Inc.

Received: December 5, 2014
Revised: March 16, 2015
Accepted: May 18, 2015
Published: July 2, 2015

REFERENCES

Bagrodia, S., Smeal, T., and Abraham, R.T. (2012). Mechanisms of intrinsic and acquired resistance to kinase-targeted therapies. Pigment Cell Melanoma Res. *25*, 819–831.

Camidge, D.R. (2013). Taking aim at ALK across the blood-brain barrier. J. Thorac. Oncol. *8*, 389–390.

Camidge, D.R., Bang, Y.J., Kwak, E.L., Iafrate, A.J., Varella-Garcia, M., Fox, S.B., Riely, G.J., Solomon, B., Ou, S.H., Kim, D.W., et al. (2012). Activity and safety of crizotinib in patients with ALK-positive non-small-cell lung cancer: updated results from a phase 1 study. Lancet Oncol. *13*, 1011–1019.

Chen, J., Jiang, C., and Wang, S. (2013). LDK378: a promising anaplastic lymphoma kinase (ALK) inhibitor. J. Med. Chem. *56*, 5673–5674.

Choi, Y.L., Soda, M., Yamashita, Y., Ueno, T., Takashima, J., Nakajima, T., Yatabe, Y., Takeuchi, K., Hamada, T., Haruta, H., et al.; ALK Lung Cancer Study Group (2010). EML4-ALK mutations in lung cancer that confer resistance to ALK inhibitors. N. Engl. J. Med. *363*, 1734–1739.

Costa, D.B., Kobayashi, S., Pandya, S.S., Yeo, W.L., Shen, Z., Tan, W., and Wilner, K.D. (2011). CSF concentration of the anaplastic lymphoma kinase inhibitor crizotinib. J. Clin. Oncol. *29*, e443–e445.

Costa, D.B., Shaw, A.T., Ignatius Ou, S.-H., Solomon, B.J., Riely, G.J., Ahn, M.-J., Zhou, C., Shreeve, S.M., Wiltshire, R., Selaru, P., et al. (2013). MO07.02 Clinical experience with crizotinib in patients with advanced ALK-rearranged non-small cell lung cancer and brain metastasis in PROFILE 1005 and PROFILE 1007. Int. J. Thorac. Oncol. *8* (*Suppl. 2*), S494–S495.

Costa, D.B., Shaw, A.T., Ou, S.H., Solomon, B.J., Riely, G.J., Ahn, M.J., Zhou, C., Shreeve, S.M., Selaru, P., Polli, A., et al. (2015). Clinical experience with crizotinib in patients with advanced ALK-rearranged non-small-cell lung cancer and brain metastases. J. Clin. Oncol. Published online January 26, 2015. http://dx.doi.org/10.1200/JCO.2014.59.0539.

Crystal, A.S., Shaw, A.T., Sequist, L.V., Friboulet, L., Niederst, M.J., Lockerman, E.L., Frias, R.L., Gainor, J.F., Amzallag, A., Greninger, P., et al. (2014). Patient-derived models of acquired resistance can identify effective drug combinations for cancer. Science *346*, 1480–1486.

Cui, J.J., Tran-Dubé, M., Shen, H., Nambu, M., Kung, P.P., Pairish, M., Jia, L., Meng, J., Funk, L., Botrous, I., et al. (2011). Structure based drug design of crizotinib (PF-02341066), a potent and selective dual inhibitor of mesenchymal-epithelial transition factor (c-MET) kinase and anaplastic lymphoma kinase (ALK). J. Med. Chem. *54*, 6342–6363.

Doebele, R.C., Pilling, A.B., Aisner, D.L., Kutateladze, T.G., Le, A.T., Weickhardt, A.J., Kondo, K.L., Linderman, D.J., Heasley, L.E., Franklin, W.A., et al. (2012). Mechanisms of resistance to crizotinib in patients with ALK gene rearranged non-small cell lung cancer. Clin. Cancer Res. *18*, 1472–1482.

Friboulet, L., Li, N., Katayama, R., Lee, C.C., Gainor, J.F., Crystal, A.S., Michellys, P.Y., Awad, M.M., Yanagitani, N., Kim, S., et al. (2014). The ALK inhibitor ceritinib overcomes crizotinib resistance in non-small cell lung cancer. Cancer Discov. *4*, 662–673.

Gadgeel, S.M., Gandhi, L., Riely, G.J., Chiappori, A.A., West, H.L., Azada, M.C., Morcos, P.N., Lee, R.M., Garcia, L., Yu, L., et al. (2014). Safety and activity of alectinib against systemic disease and brain metastases in patients with crizotinib-resistant ALK-rearranged non-small-cell lung cancer (AF-002JG): results from the dose-finding portion of a phase 1/2 study. Lancet Oncol. *15*, 1119–1128.

Gainor, J.F., and Shaw, A.T. (2013). Emerging paradigms in the development of resistance to tyrosine kinase inhibitors in lung cancer. J. Clin. Oncol. *31*, 3987–3996.

Gandhi, L., Drappatz, J., Ramaiya, N.H., and Otterson, G.A. (2013). High-dose pemetrexed in combination with high-dose crizotinib for the treatment of refractory CNS metastases in ALK-rearranged non-small-cell lung cancer. J. Thorac. Oncol. *8*, e3–e5.

Gerber, D.E., and Minna, J.D. (2010). ALK inhibition for non-small cell lung cancer: from discovery to therapy in record time. Cancer Cell *18*, 548–551.

Huang, Q., Johnson, T.W., Bailey, S., Brooun, A., Bunker, K.D., Burke, B.J., Collins, M.R., Cook, A.S., Cui, J.J., Dack, K.N., et al. (2014). Design of potent and selective inhibitors to overcome clinical anaplastic lymphoma kinase mutations resistant to crizotinib. J. Med. Chem. *57*, 1170–1187.

Ignatius Ou, S.H., Azada, M., Hsiang, D.J., Herman, J.M., Kain, T.S., Siwak-Tapp, C., Casey, C., He, J., Ali, S.M., Klempner, S.J., and Miller, V.A. (2014). Next-generation sequencing reveals a Novel NSCLC ALK F1174V mutation and confirms ALK G1202R mutation confers high-level resistance to alectinib (CH5424802/RO5424802) in ALK-rearranged NSCLC patients who progressed on crizotinib. J. Thorac. Oncol. *9*, 549–553.

Johnson, T.W., Richardson, P.F., Bailey, S., Brooun, A., Burke, B.J., Collins, M.R., Cui, J.J., Deal, J.G., Deng, Y.L., Dinh, D., et al. (2014). Discovery of (10R)-7-amino-12-fluoro-2,10,16-trimethyl-15-oxo-10,15,16,17-tetrahydro-2H-8,4-(metheno)pyrazolo[4,3-h][2,5,11]-benzoxadiazacyclotetradecine-3-carbonitrile (PF-06463922), a macrocyclic inhibitor of anaplastic lymphoma kinase (ALK) and c-ros oncogene 1 (ROS1) with preclinical brain exposure and broad-spectrum potency against ALK-resistant mutations. J. Med. Chem. *57*, 4720–4744.

Kaneda, H., Okamoto, I., and Nakagawa, K. (2013). Rapid response of brain metastasis to crizotinib in a patient with ALK rearrangement-positive non-small-cell lung cancer. J. Thorac. Oncol. *8*, e32–e33.

Katayama, R., Khan, T.M., Benes, C., Lifshits, E., Ebi, H., Rivera, V.M., Shakespeare, W.C., Iafrate, A.J., Engelman, J.A., and Shaw, A.T. (2011). Therapeutic strategies to overcome crizotinib resistance in non-small cell lung cancers harboring the fusion oncogene EML4-ALK. Proc. Natl. Acad. Sci. USA *108*, 7535–7540.

Katayama, R., Shaw, A.T., Khan, T.M., Mino-Kenudson, M., Solomon, B.J., Halmos, B., Jessop, N.A., Wain, J.C., Yeo, A.T., Benes, C., et al. (2012). Mechanisms of acquired crizotinib resistance in ALK-rearranged lung cancers. Sci. Transl. Med. *4*, 120ra17.

Katayama, R., Friboulet, L., Koike, S., Lockerman, E.L., Khan, T.M., Gainor, J.F., Iafrate, A.J., Takeuchi, K., Taiji, M., Okuno, Y., et al. (2014). Two novel ALK mutations mediate acquired resistance to the next-generation ALK inhibitor alectinib. Clin. Cancer Res. *20*, 5686–5696.

Kim, S., Kim, T.M., Kim, D.W., Go, H., Keam, B., Lee, S.H., Ku, J.L., Chung, D.H., and Heo, D.S. (2013). Heterogeneity of genetic changes associated with acquired crizotinib resistance in ALK-rearranged lung cancer. J. Thorac. Oncol. *8*, 415–422.

Kinoshita, K., Asoh, K., Furuichi, N., Ito, T., Kawada, H., Hara, S., Ohwada, J., Miyagi, T., Kobayashi, T., Takanashi, K., et al. (2012). Design and synthesis of a highly selective, orally active and potent anaplastic lymphoma kinase inhibitor (CH5424802). Bioorg. Med. Chem. *20*, 1271–1280.

Kinoshita, Y., Koga, Y., Sakamoto, A., and Hidaka, K. (2013). Long-lasting response to crizotinib in brain metastases due to EML4-ALK-rearranged non-small-cell lung cancer. BMJ Case Rep. *2013*.

Kodack, D.P., Chung, E., Yamashita, H., Incio, J., Duyverman, A.M., Song, Y., Farrar, C.T., Huang, Y., Ager, E., Kamoun, W., et al. (2012). Combined targeting of HER2 and VEGFR2 for effective treatment of HER2-amplified breast cancer brain metastases. Proc. Natl. Acad. Sci. USA *109*, E3119–E3127.

Kwak, E.L., Bang, Y.J., Camidge, D.R., Shaw, A.T., Solomon, B., Maki, R.G., Ou, S.H., Dezube, B.J., Jänne, P.A., Costa, D.B., et al. (2010). Anaplastic lymphoma kinase inhibition in non-small-cell lung cancer. N. Engl. J. Med. *363*, 1693–1703.

Lackner, M.R., Wilson, T.R., and Settleman, J. (2012). Mechanisms of acquired resistance to targeted cancer therapies. Future Oncol. *8*, 999–1014.

Lovly, C.M., McDonald, N.T., Chen, H., Ortiz-Cuaran, S., Heukamp, L.C., Yan, Y., Florin, A., Ozretić, L., Lim, D., Wang, L., et al. (2014). Rationale for co-targeting IGF-1R and ALK in ALK fusion-positive lung cancer. Nat. Med. *20*, 1027–1034.

Mager, D.E., Wyska, E., and Jusko, W.J. (2003). Diversity of mechanism-based pharmacodynamic models. Drug Metab. Dispos. *31*, 510–518.

Maillet, D., Martel-Lafay, I., Arpin, D., and Pérol, M. (2013). Ineffectiveness of crizotinib on brain metastases in two cases of lung adenocarcinoma with EML4-ALK rearrangement. J. Thorac. Oncol. *8*, e30–e31.

Rosenzweig, S.A. (2012). Acquired resistance to drugs targeting receptor tyrosine kinases. Biochem. Pharmacol. *83*, 1041–1048.

Sasaki, T., Koivunen, J., Ogino, A., Yanagita, M., Nikiforow, S., Zheng, W., Lathan, C., Marcoux, J.P., Du, J., Okuda, K., et al. (2011). A novel ALK secondary mutation and EGFR signaling cause resistance to ALK kinase inhibitors. Cancer Res. *71*, 6051–6060.

Shaw, A.T., and Engelman, J.A. (2013). ALK in lung cancer: past, present, and future. J. Clin. Oncol. *31*, 1105–1111.

Shaw, A.T., Kim, D.W., Nakagawa, K., Seto, T., Crinó, L., Ahn, M.J., De Pas, T., Besse, B., Solomon, B.J., Blackhall, F., et al. (2013). Crizotinib versus chemotherapy in advanced ALK-positive lung cancer. N. Engl. J. Med. *368*, 2385–2394.

Shaw, A.T., Kim, D.W., Mehra, R., Tan, D.S., Felip, E., Chow, L.Q., Camidge, D.R., Vansteenkiste, J., Sharma, S., De Pas, T., et al. (2014a). Ceritinib in ALK-rearranged non-small-cell lung cancer. N. Engl. J. Med. *370*, 1189–1197.

Shaw, A.T., Mehra, R., Tan, D., Felip, E., Chow, L., Camidge, D.R., Vansteenkiste, J., Sharma, S., De Pas, T., Riely, G., et al. (2014b). 1293P—Evaluation of ceritinib-treated patients (pts) with anaplastic lymphoma kinase rearranged (ALK+) non-small cell lung cancer (NSCLC) and brain metastasis. Ann. Oncol. *25* (*Suppl_4*), iv426–iv470.

Solomon, B., Felip, E., Blackhall, F., Mok, T., Kim, D., Wu, Y., Nakagawa, K., Mekhail, T., Paolini, J., Usari, T., et al. (2014a). Overall and incranial (IC) efficacy results and time to symptom deterioration in PROFILE 1014: 1st line crizotinib vs. premetrexed-platinum chemotherapy (PPC) in pateints with advanced ALK-positive non-squamous non-smeall cell lung cancer (NSCLC). Ann. Oncol. *25* (*Suppl_4*), iv426–iv470.

Solomon, B., Wilner, K.D., and Shaw, A.T. (2014b). Current status of targeted therapy for anaplastic lymphoma kinase-rearranged non-small cell lung cancer. Clin. Pharmacol. Ther. *95*, 15–23.

Solomon, B.J., Mok, T., Kim, D.W., Wu, Y.L., Nakagawa, K., Mekhail, T., Felip, E., Cappuzzo, F., Paolini, J., Usari, T., et al.; PROFILE 1014 Investigators (2014c). First-line crizotinib versus chemotherapy in ALK-positive lung cancer. N. Engl. J. Med. *371*, 2167–2177.

Taipale, M., Krykbaeva, I., Whitesell, L., Santagata, S., Zhang, J., Liu, Q., Gray, N.S., and Lindquist, S. (2013). Chaperones as thermodynamic sensors of drug-target interactions reveal kinase inhibitor specificities in living cells. Nat. Biotechnol. *31*, 630–637.

Takeda, M., Okamoto, I., and Nakagawa, K. (2013). Clinical impact of continued crizotinib administration after isolated central nervous system progression in patients with lung cancer positive for ALK rearrangement. J. Thorac. Oncol. *8*, 654–657.

Tanizaki, J., Okamoto, I., Okabe, T., Sakai, K., Tanaka, K., Hayashi, H., Kaneda, H., Takezawa, K., Kuwata, K., Yamaguchi, H., et al. (2012). Activation of HER family signaling as a mechanism of acquired resistance to ALK inhibitors in EML4-ALK-positive non-small cell lung cancer. Clin. Cancer Res. *18*, 6219–6226.

Weickhardt, A.J., Scheier, B., Burke, J.M., Gan, G., Lu, X., Bunn, P.A., Jr., Aisner, D.L., Gaspar, L.E., Kavanagh, B.D., Doebele, R.C., and Camidge, D.R. (2012). Local ablative therapy of oligoprogressive disease prolongs disease control by tyrosine kinase inhibitors in oncogene-addicted non-small-cell lung cancer. J. Thorac. Oncol. *7*, 1807–1814.

Weinstein, I.B. (2002). Cancer. Addiction to oncogenes—the Achilles heal of cancer. Science *297*, 63–64.

Yamazaki, S., Lam, J.L., Zou, H.Y., Wang, H., Smeal, T., and Vicini, P. (2014). Translational pharmacokinetic-pharmacodynamic modeling for an orally available novel inhibitor of anaplastic lymphoma kinase and c-Ros oncogene 1. J. Pharmacol. Exp. Ther. *351*, 67–76.

Zou, H.Y., Li, Q., Engstrom, L.D., West, M., Appleman, V., Wong, K.A., McTigue, M., Deng, Y.L., Liu, W., Brooun, A., et al. (2015). PF-06463922 is a potent and selective next-generation ROS1/ALK inhibitor capable of blocking crizotinib-resistant ROS1 mutations. Proc. Natl. Acad. Sci. USA *112*, 3493–3498.